

Comparison of longwave effective cloud fraction with ARM cloudiness measurements

E. E. Takara and R. G. Ellingson
The Florida State University
Department of Meteorology
Tallahassee, FL 32306-4520 USA

ABSTRACT

The longwave effective cloud fraction is derived from surface longwave measurements by pyrgeometer, interferometer, and cloud base height measurements. Results from two sets of radiance thresholds, one for low clouds and another more sensitive to high clouds, are presented and compared to the opaque total sky cover from a sky imager. With thresholds set for the low clouds there was some agreement with the sky imager for lower clouds, but agreement decreased as cloud base height increased.

When the threshold was set for high clouds there was increased high cloud detection, at the cost of overestimating cloud amounts for middle and low clouds. As with any method for cloud detection from surface longwave measurements, there are two problems. First, clouds are harder to detect as temperature and water vapor amount increases because of masking by increased gaseous emission. Second, multiple cloud layers make it difficult to determine proper threshold values for cloud detection.

1. INTRODUCTION

The Atmospheric Radiation Measurement (ARM) program is one of the climate research efforts of the United States (US) Department of Energy. As the name implies, the ARM program seeks to measure quantities relevant to atmospheric radiation, archiving measurements over time scales suitable for climate studies. ARM takes surface based measurements at sites in the US Southern Great Plains (SGP), the North Slope of Alaska (NSA), and the Tropical Western Pacific (TWP). ARM also conducts field campaigns, often in co-operation with other agencies.

The Cloudiness Intercomparison field campaign took place from February through May 2003 at the SGP Central Facility (36° N 37° 97' W 30"). Its purpose was to compare several different instruments and methods of measuring cloud amount. While it may seem to be a simple quantity, cloud amount is somewhat elusive. Different types of instruments placed within meters of each other can give different cloud amounts because they use different parts of the spectrum, have different fields of view, sampling rates, etc. Here the longwave effective cloud fraction (N_e) is described and compared to measurements from the Total Sky Imager (TSI), Long, 2003.

Another consideration is that cloud amount depends on the physical scale under consideration. The cloud amount appropriate for comparison to a single pyrgeometer is not likely to be useful for a grid square with 100km sides.

In terms of N_e , the average longwave surface flux F , over an area that is large compared to individual clouds, is $F = (1 - N_e)F_{\text{clear}} + N_e F_{\text{overcast}}$ (1) F_{clear} is the clear sky flux; the flux that would occur if the broken cloud field was removed. F_{overcast} is the flux that would occur if the broken cloud field became completely overcast. N_e is the fractional sky coverage of flat black plates.

2. INSTRUMENTS AND MEASUREMENTS

Re-arranging (1) to solve for N_e and substituting F_{pyr} for F yields:

$$N_e = \frac{F_{\text{pyr}} - F_{\text{clear}}}{F_{\text{overcast}} - F_{\text{clear}}} \quad (2)$$

In Han and Ellingson (1999) longwave parameterizations were found for cumulus cloud fields. In that study, F_{pyr} , F_{clear} , and F_{overcast} were obtained through measurements, fixing N_e . That process is used here for all skies.

Several data sets from the ARM SGP central facility were used to derive N_e . The radiances and surface emitting temperature from the Atmospheric Emitted Radiance Interferometer (AERI), Felz et al 1998, and cloud base from Active Remote Sensing of Cloud Layers (ARSCL), Clothiaux et al, 2000, were used to derive the F_{clear} and F_{overcast} throughout the day. The longwave (0-3000 cm^{-1}) downward flux, F_{pyr} , was measured directly by pyrgeometer. The resulting N_e are compared to the TSI opaque total sky cover, the fraction of the TSI hemispherical view taken up by opaque clouds.

This method is similar to that described in Durr and Philipona (2004) in that it is based on longwave surface measurements. It has the advantage of being continuous; the same algorithm is valid in daytime and nighttime. The disadvantage of surface longwave methods is that clouds become difficult to detect during the summer or in the Tropics because of larger gaseous emission due to greater water vapor amounts and higher temperatures. This increased emission masks high/cold clouds. Active measurements at other wavelengths such as radar and lidar have the advantage of being able to "illuminate" high clouds. Shortwave methods like Long and Ackerman (2000) are somewhat active, with the Sun for illumination.

3. COMPUTING F_{clear} AND F_{overcast}

The AERI takes calibrated radiance measurements of the downwelling radiance from 520 to 3020 cm^{-1} at approximately 0.5 cm^{-1} resolution. Adding the 5200 measured radiances, I_{AERI} , from 520 to 3020 cm^{-1} gives the total measured AERI radiance $I_{\text{AERI}}^{\text{tot}}$:

$$I_{\text{AERI}}^{\text{tot}} = \sum I_{\text{AERI}} \quad (3)$$

Assuming that the downwelling radiance outside the 833-1250 cm^{-1} window can be approximated by the Planck function (B_{ν}), pseudo-window radiance (I_w) can be defined as:

$$I_w = I_{\text{AERI}}^{\text{tot}} - I_{\text{opq}} \quad (4)$$

$$I_{\text{opq}} = \int_{520 \text{ cm}^{-1}}^{833 \text{ cm}^{-1}} B_{\nu}(T_s, \nu) d\nu + \int_{1250 \text{ cm}^{-1}}^{3020 \text{ cm}^{-1}} B_{\nu}(T_s, \nu) d\nu \quad (5)$$

The combination of a low standard deviation in the AERI 990 cm^{-1} radiance and a high I_w indicates the presence of clouds. If an overcast threshold radiance is used, the observed I_w is considered an overcast radiance, I_w^{overcast} , when $I_w \geq I_{\text{thold}}(\text{overcast})$. A low standard deviation and low I_w indicates clear skies. When using a clear threshold, I_w is considered to be a clear radiance, I_w^{clear} , when $I_w \leq I_{\text{thold}}(\text{clear})$. The values of $I_{\text{thold}}(\text{overcast/clear})$ change according to the surface temperature and water vapor amounts.

The clear and overcast fluxes can be computed from the I_w according to:

$$I_{\text{AERI}}^{\text{tot,clear}} = I_w^{\text{clear}} + I_{\text{opq}} \quad (6)$$

$$I_{\text{AERI}}^{\text{tot,overcast}} = I_w^{\text{overcast}} + I_{\text{opq}} \quad (7)$$

$$F_{\text{clear}} = LI_{\text{AERI}}^{\text{tot,clear}} + F_{0-520} + F_{\text{offset}} \quad (8)$$

$$F_{\text{overcast}} = LI_{\text{AERI}}^{\text{tot,overcast}} + F_{0-520} + F_{\text{offset}} \quad (9)$$

$$F_{0-520} = \pi \int_{0 \text{ cm}^{-1}}^{520 \text{ cm}^{-1}} B_{\nu}(T_{\text{surf}}, \nu) d\nu \quad (10)$$

$$F_{\text{offset}} = \delta_{\text{pyr-AERI}} \quad (11)$$

Where L is a conversion factor ranging from π at the surface to 2.45 for clear skies, F_{0-520} is the flux from the 0-520 cm^{-1} opaque spectrum not measured by the AERI, and $\delta_{\text{pyr-AERI}}$ is the instrument offset between the AERI and pyrgeometer. By iteration, clear and overcast radiances can be found and used to construct the clear and overcast flux envelopes throughout the day. Using Eq. 2, this leads to N_e .

4. COMPARING N_e TO THE TSI

Two sets of threshold radiances were used to derive N_e . In the first, clear and overcast threshold radiances $I_{\text{thold}}(\text{clear})$ and $I_{\text{thold}}(\text{overcast})$ were specified based on

monthly values. In order to increase the cloud sensitivity to only the previous clear threshold, $I_{\text{thold}}(\text{clear})$, was used.

4.1 N_e for clear and overcast threshold radiances

Figure 1 is a binned scatter plot comparing the derived TSI opaque total sky cover on the x-axis to the longwave N_e on the y-axis, for ARSCL clear sky and lowest cloud base heights (Z_b) less than 4km. The x and y points are in eleven bins, nine of width 0.1 starting at 0.05, and two of width 0.05 starting at 0 and 0.95 respectively. There will be a single diagonal line of black boxes from (0,0) to (1,1) if the N_e and TSI agree within the limits of the bins.

The N_e were derived using the first set of thresholds, using both clear and cloudy threshold radiances. This underestimates the cloud amount in most cases because some actual cloud radiances are below the cloudy threshold. The binned plot shows significant agreement at opaque TSI ≥ 0.95 . So, the longwave N_e can identify overcast low clouds. The agreement at TSI ≤ 0.05 is somewhat spurious because an overly high overcast threshold will overestimate the clear sky amount.



Fig. 1, Binned longwave N_e vs. opaque TSI for ARSCL clear and clouds with $Z_b < 4\text{km}$, clear and overcast thresholds.

Figure 2 compares the clear and overcast threshold N_e with TSI for medium clouds: $4\text{km} \leq Z_b < 8\text{km}$. Again, the N_e consistently underestimates the cloud amount. There is some agreement at opaque TSI ≥ 0.95 , but much less than for $Z_b < 4\text{km}$. This indicates that there are problems with longwave N_e as the clouds get higher.

Figure 3 shows the clear and overcast threshold N_e -TSI comparison for high clouds $Z_b \geq 8\text{km}$. This illustrates the problem with detecting higher clouds using longwave instruments. For the most part the longwave N_e shows clear skies. In fact, the number of clear sky cases is overestimated by a factor of 2.

Figure 4 is a combination of Figures 1-3, showing the comparison of clear and overcast threshold N_e for all sky conditions. The longwave N_e derived using clear and overcast thresholds underestimates the cloud amount for all Z_b .

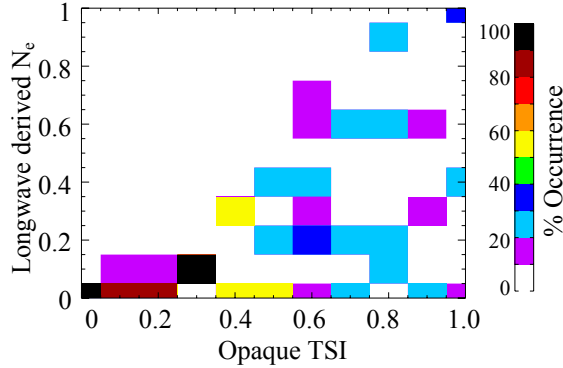


Fig. 2, Binned longwave N_e vs. opaque TSI for ARSCL clear and clouds with $4\text{km} \leq Z_b < 8\text{km}$, clear and overcast thresholds

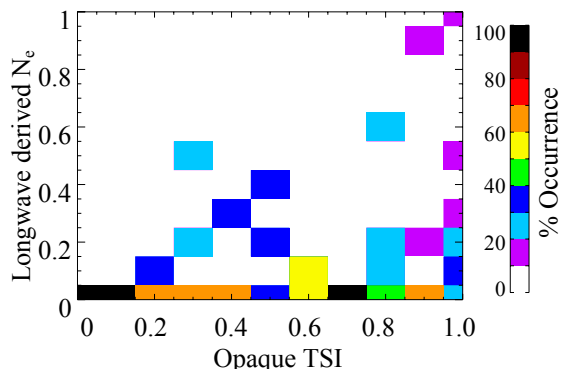


Fig. 3, Binned longwave N_e vs. opaque TSI for ARSCL clear and clouds with $Z_b \geq 8\text{km}$, clear and overcast thresholds.

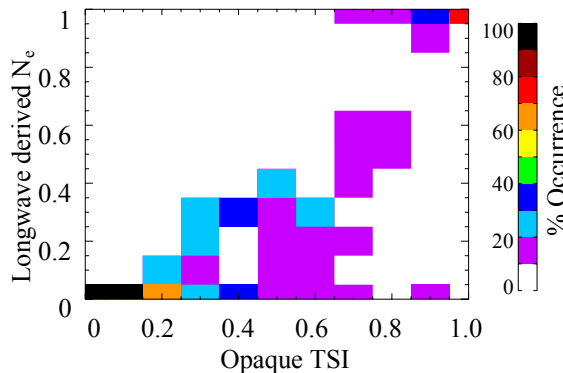


Fig. 4, Binned longwave N_e vs. opaque TSI for all skies, clear and overcast thresholds.

4.2 N_e for clear threshold radiance

Figure 5 shows the threshold clear and overcast N_e -TSI comparison for clear sky and $Z_b < 4\text{km}$ with N_e derived using only the previous clear sky threshold. This should be more sensitive to less emitting (colder or thinner) clouds. The increased sensitivity has the disadvantage of making

large clear sky radiances appear to be cloud radiances. This can be seen along the top of the figure, where there is a significant number of bins at $N_e=1$ when the opaque TSI values are less than 0.8. As before, the binned plot shows significant agreement at opaque $\text{TSI} \geq 0.95$.

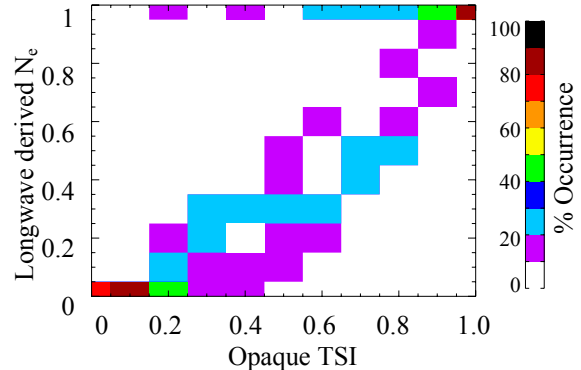


Fig. 5, Binned longwave N_e vs. opaque TSI for ARSCL clear and clouds with $Z_b < 4\text{km}$, clear

Figure 6 shows the comparison for medium clouds: $4\text{km} \leq Z_b < 8\text{km}$. The bins in Figure 6 are much more scattered than for the previous thresholds shown in Fig. 2. As with Fig. 5, this is also shows too much sensitivity, leading to overestimates of cloud amount. As stated earlier, this could be due to problems with higher clouds.

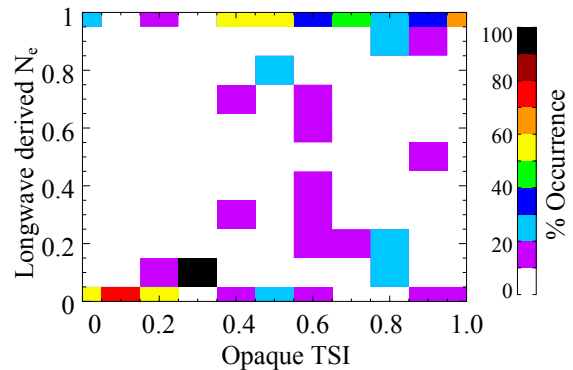


Fig. 6, Binned longwave N_e vs. opaque TSI for ARSCL clear and clouds with $4\text{km} \leq Z_b < 8\text{km}$, clear threshold.

Figure 7 shows the N_e -TSI comparison for high clouds; $Z_b \geq 8\text{km}$. It shows some success in detecting higher clouds -- the upper right quadrant is more populated than in Fig. 3. Figure 8 shows the comparison for all sky conditions.

Using only a clear sky threshold shows some improvement in detecting clouds with low emission, but the figures indicate that sensitivity to low-emitting clouds comes at the cost of overestimating the cloud amount. This may be addressed by more sophisticated thresholds for clear and overcast radiance.

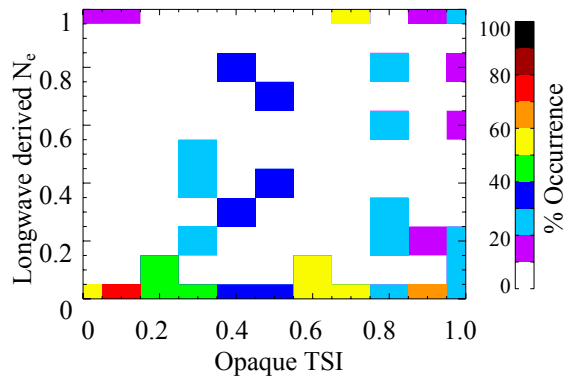


Fig. 7, Binned longwave N_e vs. opaque TSI for ARSCL clear and clouds with $Z_b \geq 8\text{km}$, clear

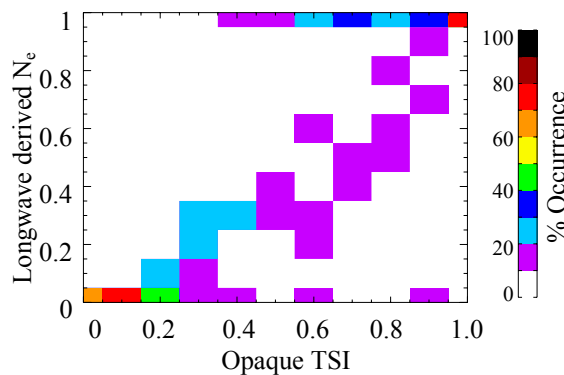


Fig. 8, Binned longwave N_e vs. opaque TSI for all skies, clear threshold.

5. SUMMARY AND CONCLUSIONS

The results from two sets of thresholds for computing effective cloud fraction (N_e) were compared with the total sky cover for opaque clouds measured by the TSI. The first set used threshold values to determine clear sky and cloud radiances. The second used only the previous clear sky threshold. The N_e found using clear and cloudy thresholds were almost always lower than the TSI opaque cloud amount. This N_e showed agreement with the TSI for clouds below 4km. The agreement between N_e and TSI decreased for middle and high clouds. The N_e found using only clear sky thresholds was more sensitive to low-emitting clouds, noticeable for the high clouds ($Z_b \geq 8\text{km}$). The increase in sensitivity caused an overestimate of cloud amount, for middle ($4\text{km} \leq Z_b < 8\text{km}$) and low clouds ($Z_b < 4\text{km}$).

As the Cloudiness Intercomparison progressed through spring and approached summer, the gaseous emission increased as the average temperature and water vapor amount increased, masking the cloud emission. Making the threshold limits more flexible will improve these results. Another related problem as the atmosphere became more active in the spring and summer was multiple cloud layers. Multiple cloud layers will require a more sophisticated algorithm which can properly maintain multiple overcast flux envelopes. Until the threshold limits can be made more flexible, this will be an awkward problem.

ACKNOWLEDGMENTS

This paper was sponsored in part by the U.S. Department of Energy's Atmospheric Radiation Measurements (ARM) program under grant DEFG0202ER63338.

REFERENCES

- Durr, B., and R. Philipona, 2004: Automatic cloud amount detection by surface longwave downward radiation measurements. *J. Geophys. Res.*, **109**, No. D5, D05201.
- Clothiaux, E. E., T. P. Ackerman, G. G. Mace, K. P. Moran, R. T. Marchand, M. Miller, and B. E. Martner, 2000: Objective determination of cloud heights and radar reflectivities using a combination of active remote sensors at the ARM CART sites. *J. of Appl. Meteor.*, **39**, 645-665.
- Felz, W. F., W. L. Smith, R. O. Knuteson, H. E. Revercomb, H. M. Woolf, and H. B. Howell, 1998: Meteorological applications of temperature and water vapor retrievals from the ground-based Atmospheric Emitted Radiance Interferometer (AERI). *J. Appl. Meteor.*, **37**, 857-875.
- Han, D. and R. G., Ellingson 1999: Cumulus cloud parameterizations for longwave radiation calculations. *J. Atmos. Sci.*, **56**, 837-851.
- Long, C. N., and T. P. Ackerman, 2000: Identification of clear skies from broadband pyranometer measurements and calculation of downwelling shortwave cloud effects. *J. Geophys. Res.*, **105**, No. D12, 15609-15626.